

# Electrochemical Preparation of Platinum Nanocrystallites with Size Selectivity on Basal Plane Oriented Graphite Surfaces

J. V. Zoval, J. Lee, S. Gorer, and R. M. Penner\*

*Institute For Surface and Interface Science, Department of Chemistry, University of California, Irvine, Irvine, California 92697-2025*

*Received: October 1, 1997; In Final Form: November 25, 1997*

Platinum nanocrystals were deposited on basal plane oriented graphite surfaces from dilute (1.0 mM)  $\text{PtCl}_6^{2-}$ -containing electrolytes using a pulsed potentiostatic method. The deposition of platinum nanocrystals occurred via an instantaneous nucleation and diffusion-limited growth mechanism which resulted in narrow particle size distributions (relative standard deviation <35%) for mean crystallite diameters smaller than 40 Å. The number of particles per unit area on these surfaces was  $10^9$ – $10^{10}$   $\text{cm}^{-2}$ . Noncontact atomic force microscopy images reveal that platinum nanocrystals nucleated both at defect sites—such as step edges—and on apparently defect-free regions of the atomically smooth graphite basal plane. Using electron transparent graphite surfaces, selected area electron diffraction analyses revealed that the structure of deposited platinum nanocrystals was fcc with a lattice constant that was indistinguishable from bulk fcc platinum. Platinum nanocrystals were not epitaxially oriented on the graphite basal plane surface.

## I. Introduction

Interest in nanoscopic platinum particles derives mostly from the importance of highly dispersed<sup>1</sup> platinum in catalysis. Many gas-phase catalytic processes exhibit a pronounced particle size dependence of the catalytic activity,<sup>2</sup> and evidence for a particle size effect in *electrochemical* reactions—such as the methanol oxidation<sup>3–5</sup> and oxygen reduction<sup>3,6–8</sup> reactions—has recently been documented. Unfortunately, progress in the area of particle size effects in electrocatalysis has been impeded by the absence of good model systems for investigating these effects. An “ideal” model system for these studies would possess all of the following characteristics: (1) Platinum nanocrystals should be size and shape monodisperse. (2) Nanocrystals should be dispersed on, and electrically connected to, a technologically relevant (and catalytically dead) support surface that facilitates spectroscopic characterization of the particles and of adsorbed intermediates. For many electrocatalysis reactions, the preferred support material is graphite. (3) Individual platinum particles on this support should be well-separated from one another. (4) The structure of the platinum nanocrystals *on the support surface* should be accessible both before and following the involvement of these particles in the catalytic process of interest. Finally, (5) platinum nanocrystallites should be *unstabilized* since functionalization of the platinum particles with a ligand layer (in order to circumvent particle aggregation) is likely to be detrimental to the electrochemical properties of the platinum particles and is therefore undesirable. Supported and unstabilized particle should be stable for days.

In this paper, we describe an electrochemical method for preparing dispersions of platinum nanocrystals on a graphite basal plane surface involving the pulsed potentiostatic deposition of platinum from dilute  $\text{PtCl}_6^{2-}$  solutions using large overpotentials ( $E_{\text{overvoltage}} \approx 500$  mV). For investigations of platinum particle size effects in electrocatalysis, the dispersions of platinum nanocrystals obtained using this method possess many,

if not all, of the desirable properties listed in the preceding paragraph, including good to excellent size monodispersity for mean particle diameters smaller than  $\approx 40$  Å. In addition, the preparation of dispersions of platinum nanocrystals is fast and convenient, and *ex situ* structural investigations of these particles using electron diffraction can be performed. Recently, we have reported that silver,<sup>9,10</sup> copper,<sup>11</sup> and cadmium nanocrystals,<sup>12</sup> which are narrowly dispersed in size, may be deposited on graphite basal plane surfaces using variants of this approach. As compared with these previous experiments, however, an additional complication in the case of platinum is that platinum nanocrystals are *spontaneously* formed at freshly cleaved HOPG surfaces that are exposed (at open circuit) to dilute  $\text{PtCl}_6^{2-}$  solutions containing no thermodynamically accessible oxidants. The thermodynamic driving force for electroless platinum deposition apparently derives from the reaction of incompletely oxidized functionalities existing at defects on the graphite surface. The preparation of platinum nanocrystals which are narrowly distributed in size requires that the spontaneous deposition of platinum be suppressed by anodically protecting the graphite surface both before and following the application of a potentiostatic pulse to the graphite surface.

Previously, supported metal nanoparticles have usually been obtained by one of the following three methods: (1) the collection of metal colloid particles from suspensions onto a surface either by controlled adsorption<sup>13–17</sup> or by electrophoresis,<sup>18–20</sup> (2) the evaporation of metal at low coverage onto a surface in a vacuum,<sup>21,22</sup> and (3) the gas-phase reduction of metal salt particles disposed on a graphite surface by  $\text{H}_2$ .<sup>23</sup> For preparing supported platinum nanoparticles for investigations of electrocatalysis, none of these three methods have proven to be entirely satisfactory: The advantage of the first approach—the collection onto a surfaces of platinum colloid particles from a suspension—is that platinum sols having good particle size monodispersity can be prepared using literature methods.<sup>24–27</sup> However, the surfaces of stabilized colloidal platinum particles are functionalized with a ligand that may have a detrimental

\* Address correspondence to this author: rmpenner@uci.edu.

effect on the electrocatalytic activity of the particle. In addition, the controlled adsorption method typically relies on a "sticky" layer on the electrode surface composed of, for example, a thiol monolayer,<sup>13,14</sup> and this layer imposes an added and undesirable electrical resistance between collected colloid particles and the electrode surface. The last two methods have the potential to yield nanocrystals that are disposed in direct contact with a substrate surface; however, in neither case has it been possible to achieve good particle size monodispersity for platinum across a wide range of particle sizes.

Electrochemical deposition has been used in several previous cases to obtain micron-scale platinum particles,<sup>28–30</sup> and nanometer-scale platinum particles have been observed in STM investigations of platinum nucleation and growth on graphite<sup>31</sup> and on semiconductor surfaces;<sup>32,33</sup> however, dispersions of supported, size-similar platinum nanocrystals have not been obtained by electrochemical methods in any previous study. An electrochemical method has, however, been developed for preparing nanoscopic palladium particles and has recently been described by Reetz and Helbig,<sup>34</sup> but the resulting particles do not persist in contact with the electrode surface following synthesis, and a suspension of THF-stabilized Pd colloids is obtained.

## II. Experimental Section

The electrochemical deposition of platinum on highly oriented pyrolytic graphite basal plane surfaces was performed in a glass and Kel-F cell in which an O-ring exposed a 0.1046 cm<sup>2</sup> circular area of the graphite surface to a N<sub>2</sub>-sparged plating solution of aqueous 1.0 mM hexachloroplatinic acid (Aldrich, 99.999%) and 0.10 M hydrochloric acid (Fisher, >99.95%). This solution was prepared using Nanopure water ( $\rho > 18 \text{ M}\Omega \text{ cm}^{-1}$ ). A saturated calomel reference electrode (SCE) or a saturated mercurous sulfate reference electrode (MSE) and a platinum wire counter electrode were employed for all electrochemical experiments; all potentials in this paper are, however, reported versus the MSE for purposes of simplicity. Platinum deposition was effected by immersing the graphite electrode into the platinum plating solution at a potential in the range from +140 to 200 mV vs MSE (a potential at which electroless platinum deposition was not observed), stepping the potential of the graphite surface from this initial value to a deposition potential of -600 mV. Following the application of the deposition pulse, the electrode potential was returned to +140 to 200 mV vs MSE, and the working electrode was removed from the plating solution. Note that both the immersion of the graphite electrode and the emersion of the electrode at the conclusion of the plating experiment must be carried out with this electrode potentiostated at +140 to 200 mV vs MSE. This pulse train was applied using a computer-controlled EG&G Princeton Applied Research 270M. The coulometric loading of platinum,  $Q_{\text{Pt}}$ , was taken to be the charge integrated from the onset of the potentiostatic pulse, corrected for double-layer charging in a PtCl<sub>6</sub><sup>2-</sup>-free electrolyte.

Noncontact AFM experiments in air were performed using a commercial instrument (Park Scientific Instruments (PSI Inc.) AutoProbe cp). This instrument operates in the slope-detected mode. Cantilevers were 2.0  $\mu\text{m}$  thick Ultralevers (PSI Inc.) having a force constant of 18 N/m, a resonance frequency near 300 kHz, and a nominal tip radius of 100  $\text{\AA}$ . The cantilever excitation frequency employed for these measurements was adjusted to be near the maximum slope of the cantilever resonance response curve. A free-space amplitude of cantilever motion (far from the surface) of  $\approx 5 \text{ \AA}$  was employed, and the

cantilever amplitude was damped to  $\approx 1 \text{ \AA}$  during imaging. The piezotube employed for these investigations was calibrated in the direction perpendicular to the surface using graphite basal plane surfaces on which monatomic steps were introduced by heating in flowing O<sub>2</sub> in a tube furnace at 650 °C for 2–3 min. Lateral calibration of the piezotube was performed by atomic resolution imaging of HOPG and Au(111). Following electrochemical deposition of platinum on a graphite surface, the surface was removed from the plating solution and rinsed briefly in a stream of Nanopure water. The surface was then allowed to dry in a desiccator prior to examination with the NC-AFM. Transmission electron microscopy and selected area electron diffraction data were acquired on Pt nanocrystallites without removing these nanoparticles from the graphite basal plane surface. This was accomplished by transferring thin (100–400  $\text{\AA}$  thick) HOPG flakes ( $\sim 1 \text{ mm}^2$ ) from a working electrode, on which Pt nanocrystals had been deposited either electrochemically or electroless, onto a carbon-coated gold grid (TedPella). The electrochemical and electroless deposition of Pt was then performed on this electrode using the same procedure as described above. The Pt coverage could not be determined in these experiments because Pt deposition occurs both on the TEM grid and on the carbon flake. TEM data were obtained on a Philips EM-200 microscope using an accelerating voltage of 200 keV. Diffraction patterns were obtained at a camera length of 1000 mm using a selected area aperture having a diameter of 10  $\mu\text{m}$ .

## III. Results and Discussion

**A. Electroless Platinum Deposition.** Initial attempts to prepare platinum nanocrystals using the pulsed potentiostatic method described earlier<sup>9</sup> produced disappointing results in terms of the particle size monodispersity which was obtained. Control experiments soon revealed that—in contrast to the case with silver—platinum deposition was occurring on the graphite basal plane surface in the absence of an applied potential (i.e., at open circuit). The platinum nanocrystals produced via this "electroless" route are not uniformly distributed on the graphite basal plane surface but instead are "concentrated" at the tops of step edges. This inhomogeneity in the distribution of deposited platinum is best seen in noncontact atomic force microscope (NC-AFM) images of the graphite basal plane, such as those shown in Figure 1. In Figure 1A is shown a single atomic step, 3.3  $\text{\AA}$  in height, which is decorated with a high density of Pt particles above the step. These Pt nanoparticles are approximately 25  $\text{\AA}$  in height; below the step, fewer particles are seen. Figure 1B shows a second structural feature—a "mesa"—consisting of several graphite layers disposed as narrow strips on the surface. In this case, the total height of this mesa is more than 20  $\text{\AA}$ . On graphite surfaces that had been exposed to the platinum plating solution, these strips were always observed to be heavily decorated with platinum deposits whereas fewer deposits were seen in adjacent regions of the surface, away from these mesas. In the NC-AFM image of Figure 1, these platinum deposits are ring-shaped and possess a height of  $\approx 20 \text{ \AA}$ . The beaded appearance of some of these rings suggests that these structures are formed by the aggregation of platinum nanoparticles—as reported in one previous study.<sup>35</sup>

That the particles seen in NC-AFM images such as those of Figure 1A are composed of platinum metal is readily verified by allowing the electroless deposition reaction to occur on thin (400  $\text{\AA}$  thick) electron transparent graphite flakes which permit the observation of particles by transmission electron microscopy (TEM) and the analysis of these particles by selected area

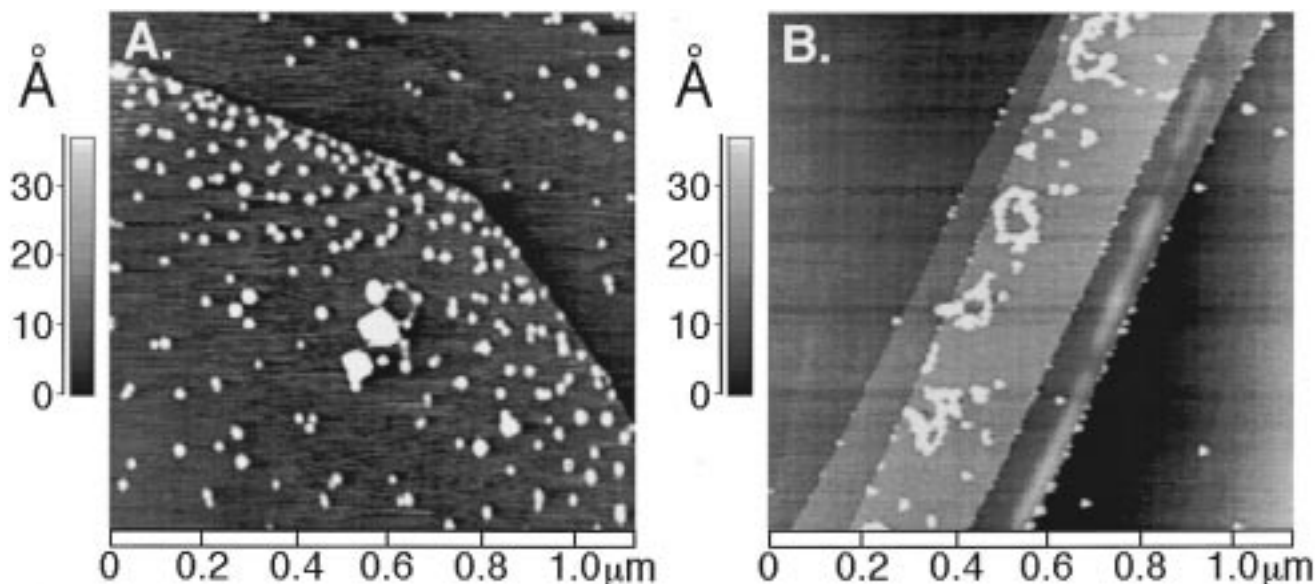
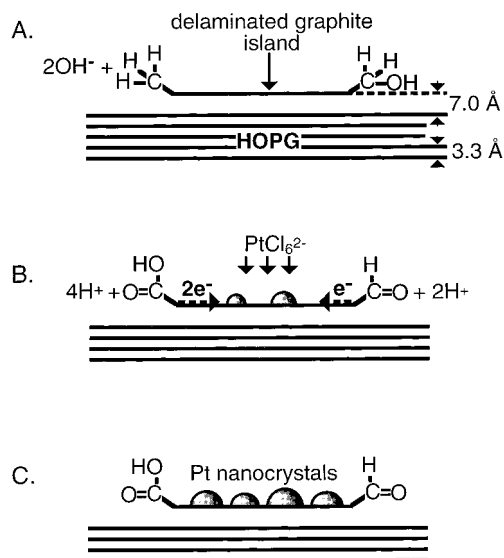


**Figure 1.** Noncontact atomic force microscope images of the graphite basal plane surface following immersion in 1.0 mM  $\text{PtCl}_6^{2-}$ , 0.10 M HCl for  $\approx 1.0$  min. Platinum nanocrystallite deposition is concentrated at the top of step edges in both images.

electron diffraction (SAED). In one typical experiment, a graphite surface was exposed to the 1.0 mM  $\text{PtCl}_6^{2-}$ , 0.10 M HCl platinum plating solution at open circuit for  $\approx 2$  min. TEM analysis of this surface revealed particles smaller than 5 nm in diameter, and electron diffraction analysis of these regions showed diffuse rings located at  $d$  spacings that are characteristic of fcc platinum (vide infra).

An open question regarding the spontaneous deposition of platinum involves the origin of the thermodynamic driving force responsible for the reduction of platinum at the graphite surface since no thermodynamically accessible sacrificial oxidants are present in the platinum plating solution to which these surfaces were exposed. Our hypothesis, based on the observed inhomogeneity of the platinum nanocrystal distribution, is that the necessary reducing equivalents are supplied by incompletely oxidized functionalities—such as aldehydes, alcohols, and ketones—existing at step edges and other defects on the graphite surface. Although the step edges at which these functionalities are concentrated are present at a very low coverage on HOPG surfaces, Raman scattering peaks have been assigned to carbonyl-containing functionalities in one recent surface-enhanced Raman spectroscopic (SERS) investigation of thermally pitted HOPG surfaces.<sup>10</sup> Schematically, the situation would then be as depicted in Scheme 1. In Scheme 1A is shown a delaminated graphite layer for which the layer spacing is greater than the normal van der Waals distance of 3.3 Å. Evidence for the delamination of surface layers is frequently seen on graphite; the “strips” shown in the NC-AFM image of Figure 1C (which exhibit an apparent height of 20 Å) provide but one example. One effect of the delamination of a graphite island may be to electrically isolate the island from the surrounding graphite surface, and under these circumstances, electrons derived from functionalities at the edges of this layer would be retained within the layer, and the reducing equivalents associated with these electrons will be available for the reduction of platinum at the surface of this layer which is exposed to the platinum plating solution (Scheme 1B). In this eventuality, platinum nanocrystals would be obtained atop an electrically isolated island, but not on the graphite surface immediately adjacent to this island—qualitatively as seen in this study. Of course, for islands that are not well isolated from the surface—such as that seen in the 3.3 Å high step edge seen in the NC-AFM image of Figure

### SCHEME 1



1A—some platinum deposition would be expected to occur adjacent to the layer as well as atop the layer—qualitatively as seen in the image of Figure 1A. While the hypothesis represented by Scheme 1 is still the subject of investigation, we have already confirmed that electrochemical preoxidation of the graphite surface (+1.0 V vs MSE for 20 s in 0.1 M  $\text{H}_2\text{SO}_4$ ) prior to exposure to the plating solution (for 45–60; 1.0 mM  $\text{PtCl}_6^{2-}$ , 0.10 M HCl) dramatically reduces the quantity of platinum that is deposited during subsequent open circuit exposure to the platinum plating solution. Scheme 1, however, fails to explain why silver, with a more positive reduction potential than  $\text{PtCl}_6^{2-}$  (0.799 and 0.74 V vs NHE, respectively), is not electrolessly deposited on HOPG surfaces.<sup>9</sup>

Of course, the spontaneous deposition of platinum on graphite must be suppressed if good particle size monodispersity is to be obtained via the potentiostatic pulse method of particle growth described previously.<sup>9</sup> In principle, the spontaneous growth of platinum can be prevented by preoxidizing the graphite surface as already indicated above. However, we have achieved even better results by anodically protecting the graphite surface at a potential of +140–200 mV vs MSE (i.e.,  $\approx 200$

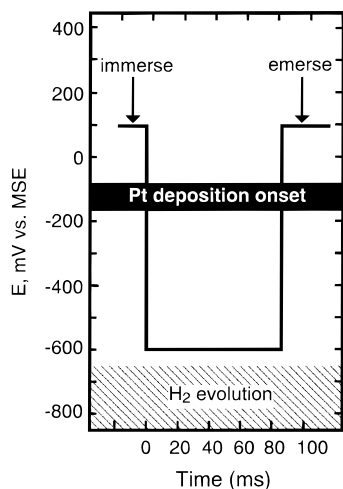


**Figure 2.** Waveform employed to effect the pulsed potentiostatic deposition of platinum nanocrystals in this study. The duration of the negative-going segment of the pulse was varied between 50 and 200 ms in this study.

mV positive of the onset for platinum deposition). For example, NC-AFM images (not shown) of graphite surfaces that were exposed to a platinum plating solution (1.0 mM  $\text{PtCl}_6^{2-}$ , 0.10 M HCl) for  $\approx 1$  min while the surface was anodically protected in this way show fewer than 10 particles, on average, in a  $3.0 \times 3.0 \mu\text{m}$  image window. This level of protection was achievable provided the graphite surface was potentiostated at all times during its exposure to the platinum plating solution.

**B. Pulsed Potentiostatic Deposition of Platinum.** The waveform shown in Figure 2 was used to effect the pulsed potentiostatic deposition of platinum nanoparticles on the graphite basal plane surface. As indicated, the graphite surface was anodically protected at +140 mV vs MSE during immersion and prior to the application of a -600 mV plating pulse. At the conclusion of the plating pulse, the potential of the surface was returned to +140 mV for a few seconds as the electrode was removed from the plating solution. The amplitude of this pulse was limited to -600 mV by the onset of  $\text{H}_2$  evolution at  $\approx 650$ –700 mV as shown in Figure 6; the duration of the plating pulse varied from 50 to 300 ms in these experiments.

A typical current–time transient seen for a 200 ms pulse in the 1.0 mM  $\text{PtCl}_6^{2-}$ , 0.10 M HCl plating solution is shown in Figure 3. The current in this time regime is linear with  $\text{time}^{-1/2}$  (see inset), consistent with a simple Cottrellian decay indicative of planar diffusion control. The Cottrell equation can be used in conjunction with the known electrode area and concentration of  $\text{PtCl}_6^{2-}$  to extract a diffusion coefficient from the slope of this linear plot;<sup>36</sup> this analysis yields a diffusion coefficient for  $\text{PtCl}_6^{2-}$  of  $5.89 \times 10^{-6} \text{ cm}^2 \text{ s}^{-1}$ , which is close to  $D$  values for this complex reported previously (e.g.,  $D_{\text{PtCl}_6^{2-}} = 4.5 \times 10^{-6} \text{ cm}^2 \text{ s}^{-1}$ ).<sup>37</sup> In conjunction with the NC-AFM and diffraction data to be presented next, this transient can be unambiguously attributed to the growth on the graphite surfaces of an ensemble of platinum nanocrystals by an instantaneous nucleation and radial diffusion-limited growth mechanism. A purely capacitive current transient was seen for the reverse (i.e., positive-going) step, qualitatively as expected based on the irreversible nature of platinum electrodeposition.

Following the deposition of platinum using the potentiostatic pulse of Figure 2, platinum nanocrystals may be directly observed by ex situ examination of the surface using NC-AFM. In Figures 4, 5, and 6 are shown NC-AFM data for surfaces on which the quantity of electrodeposited platinum was  $4.84 \mu\text{C}$

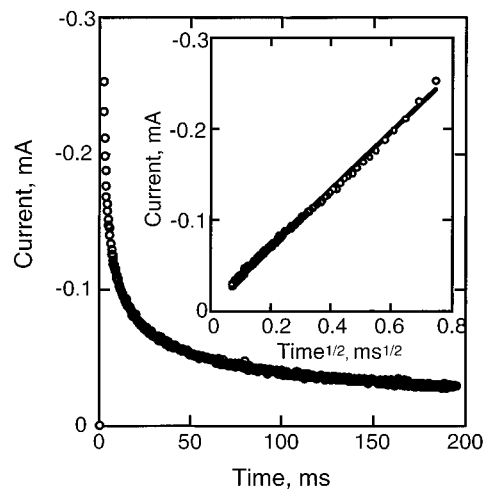


**Figure 3.** Typical current–time transient acquired at a  $0.713 \text{ cm}^2$  graphite surface in 1.0 mM  $\text{PtCl}_6^{2-}$ , 0.10 M HCl associated with the deposition of platinum nanocrystals on graphite. This transient was processed by the subtraction of a small ( $< 1\%$ ) capacitive background current. Inset: plot of current versus  $\text{time}^{-1/2}$  showing linear behavior consistent with the predictions of the Cottrell equation. A calculation of the diffusion coefficient from these data yielded a value of  $5.89 \times 10^{-6} \text{ cm}^2 \text{ s}^{-1}$ .

$\text{cm}^{-2}$  (or 0.0050 equivalent monolayers),  $37.6 \mu\text{C cm}^{-2}$  (0.039 equivalent monolayers), and  $77.1 \mu\text{C cm}^{-2}$  (or 0.080 equivalent monolayers), respectively. These three coverages were obtained by varying the deposition time from 10 ms (Figure 4) to 100 ms (Figure 6); monolayer coverages were estimated from the deposition charge assuming an adsorption electrovalency of 4.0, which yields  $964.5 \mu\text{C cm}^{-2}$  for one platinum monolayer. Three aspects of these NC-AFM images are of interest. First, the nucleation and growth of platinum particles has occurred both at step edges on the surface and on terraces where no defects are seen in the NC-AFM images. A preference for nucleation at step edges is, however, apparent in these images. Second, in contrast to the case for platinum NCs prepared by electroless deposition, no evidence for aggregation of platinum nanoparticles is seen in the NC-AFM data; platinum particles prepared by the pulsed potentiostatic method are well separated from one another on the graphite surface. Third, the coverage of particles on each of the three surfaces is approximately the same and in the range from  $3 \times 10^9$  to  $6 \times 10^9 \text{ cm}^{-2}$ . Finally, the platinum particles in Figures 4–6 possess reasonably good size monodispersity: The statistics for the particle height on these surfaces were  $25 \pm 9 \text{ \AA}$  (36% RSD),  $52 \pm 9 \text{ \AA}$  (17% RSD), and  $72 \pm 27 \text{ \AA}$  (38% RSD). In general, however, size distributions for platinum nanocrystal dispersion were much broader for large particles (diameter  $> 40 \text{ \AA}$ ) than for smaller particles. This trend is readily apparent in the particle size histograms shown in Figure 7.

The nucleation density of  $(3\text{--}6) \times 10^9 \text{ cm}^{-2}$  determined from NC-AFM images translates into an average distance between platinum particles on the surface of between 2000 and 1400  $\text{\AA}$ , respectively. This nearest-neighbor spacing accounts for the planar diffusion-controlled response seen in the current transient of Figure 3: The onset of diffusion layer overlap for adjacent platinum particles on the graphite surface will occur at a time,  $\tau \approx r^2/2D$ , where  $r$  is one-half the distance between nearest platinum particles on the surface. For  $r = 1000 \text{ \AA}$  ( $1.0 \times 10^{-5} \text{ cm}$ ) and  $D = 6.0 \times 10^{-6} \text{ cm}^2 \text{ s}^{-1}$ , overlap occurs at 8  $\mu\text{s}$ , and at somewhat longer times, the coalescence of the many radial diffusion fields about each platinum particle can be expected to yield a single planar diffusion field. Consequently, platinum

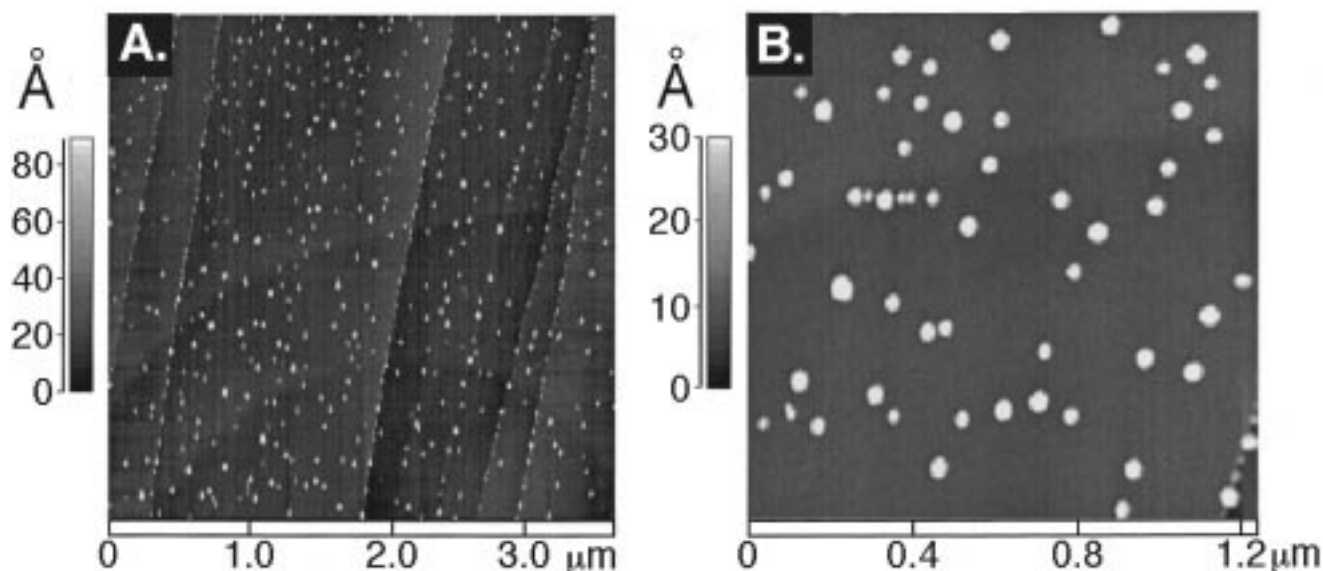


**Figure 4.** Noncontact atomic force microscope images— $3.4 \times 3.4 \mu\text{m}$  (A) and  $1.2 \times 1.2 \mu\text{m}$  (B)—of the graphite basal plane surface following the application of a 10 ms platinum pulse. A deposition charge of  $4.84 \mu\text{C cm}^{-2}$  was obtained corresponding to 0.0050 equivalent platinum atomic layers (assuming an adsorption electrovalency of 4.0). The mean particle height on this surface was  $25 \pm 9 \text{ \AA}$ .

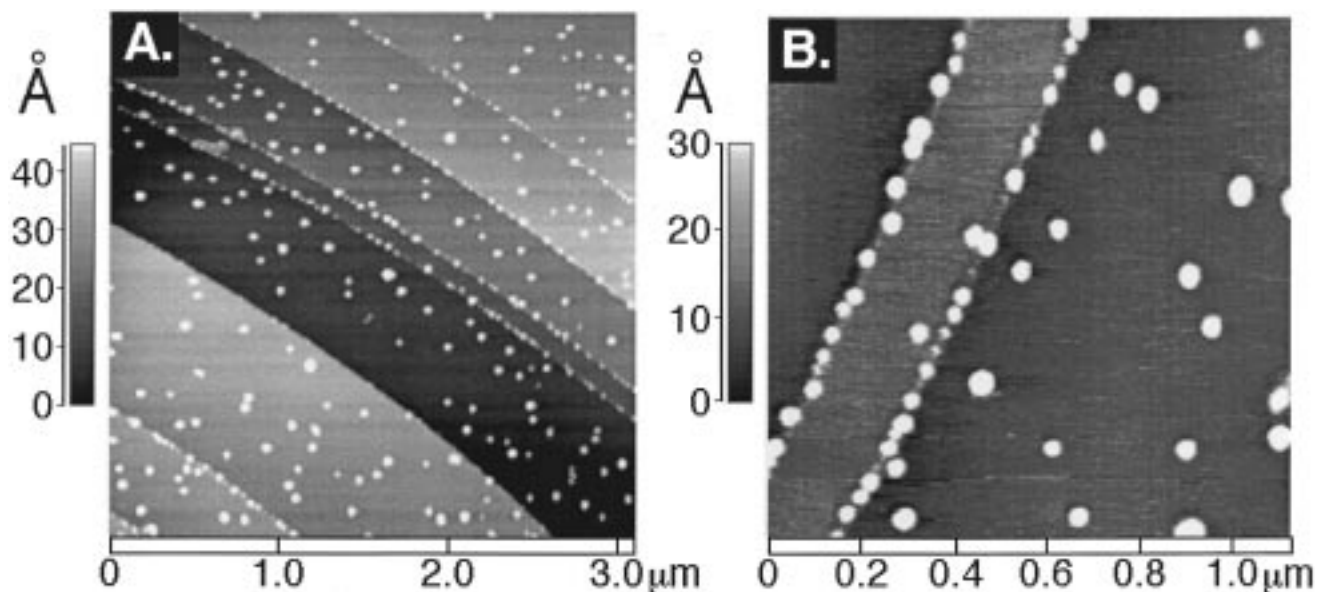


**Figure 5.** Noncontact atomic force microscope images— $3.0 \times 3.0 \mu\text{m}$  (A) and  $1.1 \times 1.1 \mu\text{m}$  (B)—of the graphite basal plane surface following the application of a 50 ms platinum pulse. A deposition charge of  $37.6 \mu\text{C cm}^{-2}$  was obtained corresponding to 0.039 equivalent platinum atomic layers. The mean particle height on this surface was  $52 \pm 9 \text{ \AA}$ .

deposition current transients like that of Figure 3 show a purely Cottrellian response. In principle, if the microsecond time domain were experimentally accessible, then a rising portion of the transient that is linear with  $t^{1/2}$  would also be observed at times shorter than  $\tau = 8 \mu\text{s}$  as predicted theoretically.<sup>38,39</sup>

It is important to emphasize here that the platinum particles obtained by pulsed potentiostatic deposition could not be observed using either scanning tunneling microscopy (STM) or conventional repulsive mode AFM imaging of the surface, even when the least perturbative imaging conditions (i.e., very low tunneling currents in STM; small applied forces in AFM) are employed. This was also true for platinum particles obtained by electroless deposition (*vide supra*). We therefore conclude that these platinum particles are weakly physisorbed on the graphite surface and that in the case of the STM and AFM experiments interactions with the tip cause the removal of these particles from the imaged area of the surface. The requirement

that a noncontact imaging experiment be employed for particle characterization may explain why dispersions of platinum nanocrystals similar to those seen in the NC-AFM images of Figures 4–6 have not been seen in any previously published study, including an electrochemical investigation platinum deposition on graphite using STM.<sup>37</sup>

Evidence that the particles seen in NC-AFM images of the graphite surface are platinum is obtained, again, from selected area electron diffraction (SAED) in conjunction with transmission electron microscopy (TEM) imaging of very thin graphite electrode surfaces. Two sets of data are shown in Figure 8: In parts A and B are shown TEM and SAED data for a surface on which  $\approx 50 \text{ \AA}$  diameter particles were deposited. This surface is qualitatively similar to that seen in the NC-AFM images of Figure 5. The corresponding SAED pattern of Figure 8B shows concentric rings, each of which possess  $d$  spacings corresponding to [111], [200], [220], and [311] of fcc platinum (International

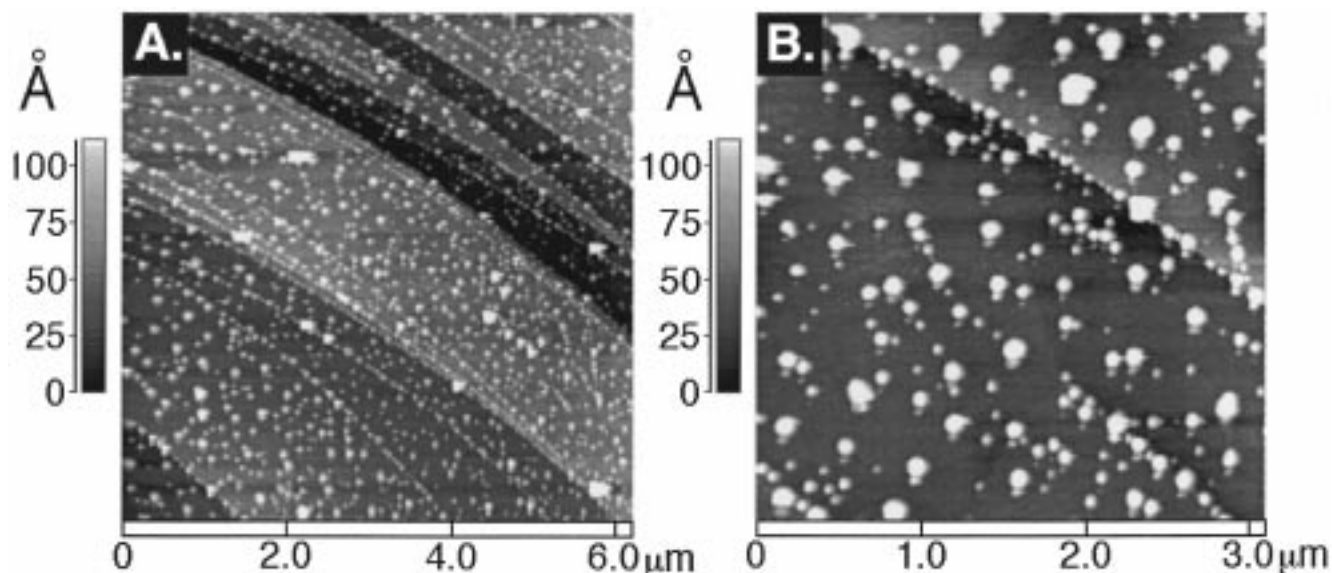


**Figure 6.** Noncontact atomic force microscope images— $6.0 \times 6.0 \mu\text{m}$  (A) and  $3.0 \times 3.0 \mu\text{m}$  (B)—of the graphite basal plane surface following the application of a 100 ms platinum pulse. A deposition charge of  $77.1 \mu\text{C cm}^{-2}$  was obtained corresponding to 0.080 equivalent platinum atomic layers. The mean particle height on this surface was  $72 \pm 27 \text{ \AA}$ . In both of these images, a “double tip” imaging artifact, manifest as a smaller “particle” observed below each larger one, is present.

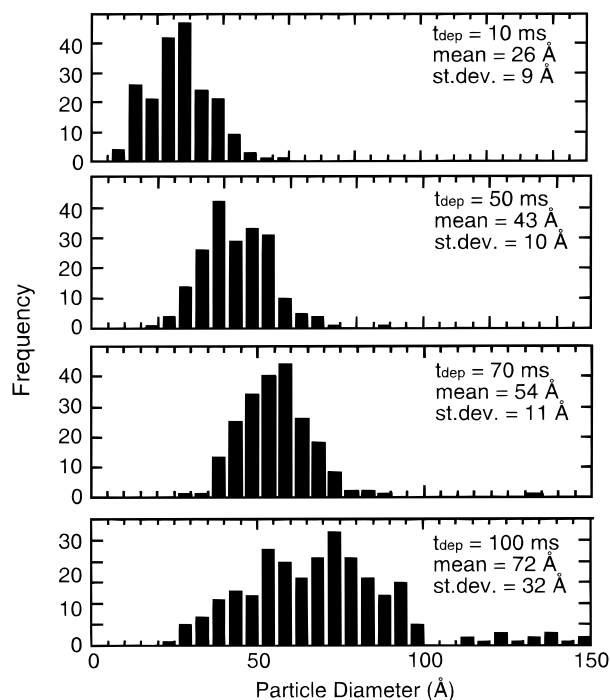


**Figure 7.** Histograms of particle heights obtained from analyses of NC-AFM images. Data for four different surfaces prepared using the conditions specified on the diagram.

Centre for Diffraction Data, #04-0802). The second pair of data (Figure 8C,D) show a graphite surface on which much larger platinum nanocrystals, up to  $500 \text{ \AA}$  in diameter, have been deposited. In the TEM image of Figure 8C, the shapes of these particles are readily discernible, and triangles, squares, and truncated triangles are observed in approximately equal numbers together with irregular shapes. The square particles represent nanocrystals having a cubic shape which exposes predominantly (100) facets,<sup>27</sup> triangular shapes can be assigned to Pt nanocrystallites having a tetrahedral geometry which exposes (111) facets,<sup>40</sup> and truncated triangles (or hexagons) are expected for cuboctahedral platinum nanocrystallites the surfaces of which expose both (100) and (111) facets.<sup>40</sup> With respect to the variety

of shapes that are observed, these TEM images are similar to those published recently by Henglein et al.<sup>25</sup> for stabilized platinum particles ( $10\text{--}30 \text{ \AA}$  in diameter) prepared by the radiolytic reduction of  $\text{PtCl}_4^{2-}$  in aqueous solution. The SAED pattern of Figure 8D again shows concentric rings corresponding to the  $d$  spacings [111], [110], and [200] of fcc platinum.

The conclusions following from the TEM and electron diffraction data are as follows: First, the particles resulting from potentiostatic pulse deposition from  $1.0 \text{ mM PtCl}_6^{2-}$ ,  $0.10 \text{ M HCl}$  plating solution, and seen in TEM and NC-AFM images of the graphite surface, are composed of fcc platinum. Second, platinum particles prepared on graphite by the potentiostatic pulse method are stable in air for days. In other words, fcc Pt diffraction is obtained from these surfaces following exposure of the surface to air for days; diffractions that are assignable to platinum oxides are not observed. This is not the case for silver nanocrystals prepared using the same potentiostatic pulse method. Third, ensembles of platinum particles always yield rings of diffracted electron intensity—never single-crystal diffraction patterns. Thus, Pt particles prepared by the potentiostatic pulse method are not epitaxially oriented on the graphite surface. In fact, no evidence for a substrate influence on the particle orientation on the surface exists. Finally, a variety of shapes are seen for platinum nanocrystals prepared by this method; the thermodynamically favored cuboctahedron is seen for just  $\approx 5\%$  of all large (diameter  $> 50 \text{ \AA}$ ) Pt nanocrystals we examined by TEM.

These last two conclusions suggest that platinum nanocrystals prepared by the potentiostatic pulse method differ in two important ways from graphite-supported platinum nanocrystals prepared by the gas-phase reduction of  $\text{H}_2\text{PtCl}_6$  at high temperatures. In two TEM studies of Pt particles obtained by gas-phase reduction of  $\text{H}_2\text{PtCl}_6$  at  $850 \text{ }^\circ\text{C}$  by Dominguez and Yacaman,<sup>41,42</sup> a cuboctahedral geometry was observed for most platinum nanocrystals, and a strong substrate influence on the orientation of these nanocrystals on the graphite basal plane was observed. It is therefore interesting to ask whether low-energy coincidences exist for any azimuthal orientations of the low index planes of a platinum nanocrystal on the hexagonal graphite surface. To address this question, we have calculated

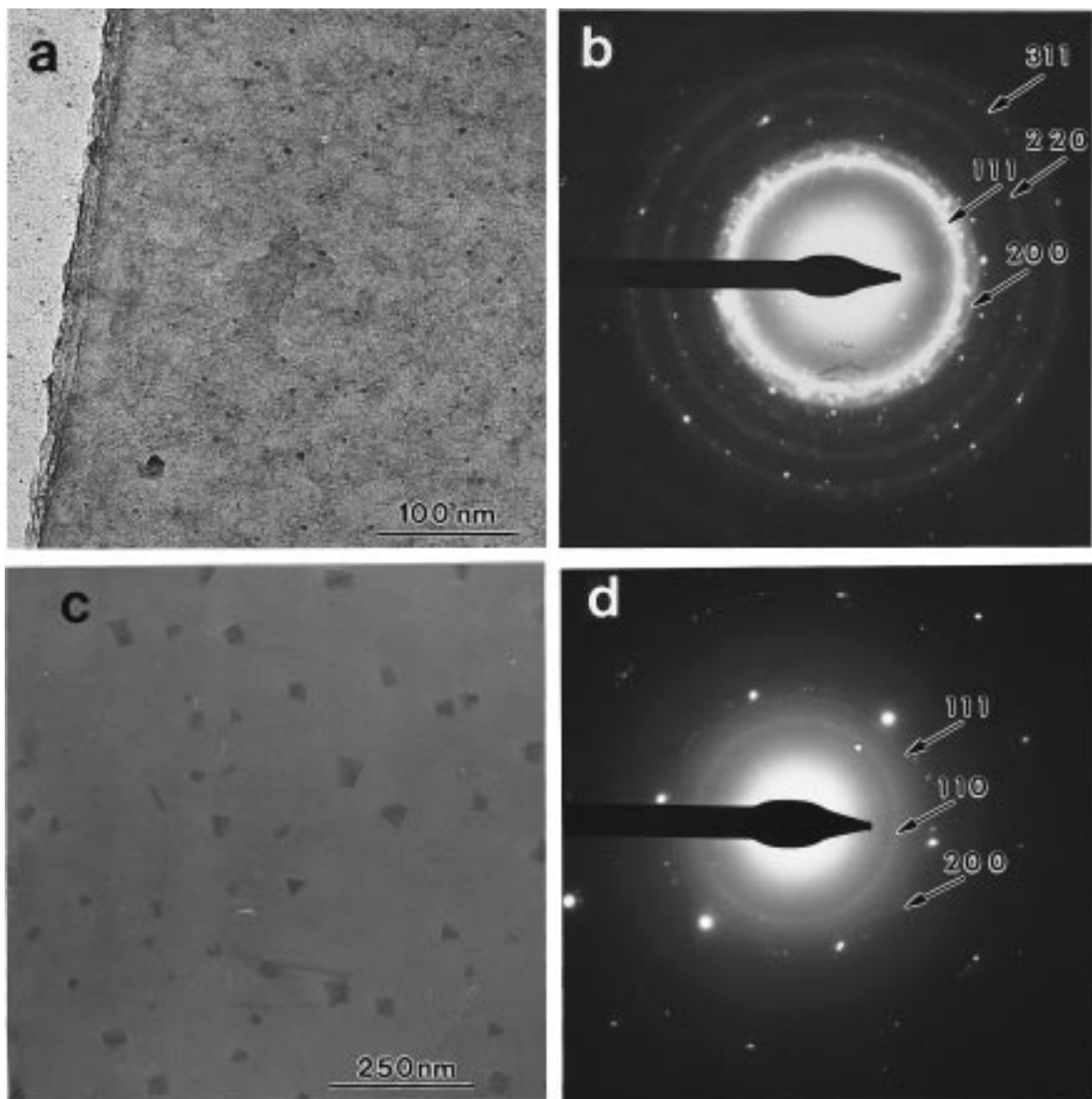


**Figure 8.** Transmission electron microscope images (a, c) of platinum nanocrystals prepared in 1.0 mM  $\text{PtCl}_6^{2-}$ , 0.10 M HCl using a deposition times of 200 ms (a) and 2 s (c). Also shown are selected area electron diffraction patterns, (b, d) for these two surfaces which were acquired for 10  $\mu\text{m}$  diameter regions centered on the two regions shown in (a) and (c), respectively. The assignments of these two patterns are as indicated.

the interaction energy for two-layer platinum fcc nanocrystals (120–150 atoms, diameter  $\approx 20$  Å) on a two-layer-thick graphite surface (1882 atoms) using a simple Lennard-Jones 6–12 potential (with  $\epsilon_0 = 350$  K and  $\sigma = 2.0$  Å) as a function of the azimuthal angle of the nanocrystal on the graphite surface. Since the L–J potential used for this calculation is not parametrized for the platinum–graphite interaction (these parameters do not exist), a reduced energy,  $E/\epsilon_0$ , is compared in Figure 9. The starting point for these calculations (i.e., angle  $0^\circ$ ) for each orientation of the platinum nanocrystal is shown in Figure 9B–D; from this initial position, the overlayer was rotated counterclockwise about the center of mass of the particle. In addition to calculations for all three low index planes of platinum, the energy of (111)-oriented faces of wurtzite CuI and CdS nanocrystals on graphite was also calculated using the same potential and plotted as a function of the angle of rotation on the surface. These two sets of data are included because we have already established<sup>11,12</sup> that CuI and CdS nanocrystals prepared by electrochemical/chemical deposition on graphite both adopt an epitaxial orientation on the graphite surface corresponding to an angle of rotation of  $30^\circ$ —and the global

energy minimum—seen in the plot of Figure 9. The main conclusion of these calculations is that none of the platinum low index faces match up with the graphite surface as well as either CuI or CdS. A Pt(110) facet shows the strongest preference for azimuthal angles of approximately  $5^\circ$  and  $65^\circ$ ; however, the 110 face possesses such low coordination that it is unlikely that this surface would provide an energetically stable facet on the surface of a platinum nanocrystal. The implication, then, is that unlike platinum nanocrystals prepared at high temperature by gas-phase chemical reduction, platinum nanocrystals synthesized electrochemically at room temperature are not able to locate the adsorption sites on the graphite surface that correspond to the shallow minima seen in Figure 9.

For the mechanism of platinum nanocrystallite nucleation and growth, two limiting cases can be distinguished: instantaneous nucleation and progressive nucleation. If nucleation is instantaneous, the number of nuclei present on the surface at any time following the onset of a deposition plating pulse will be a constant. In the progressive nucleation case in contrast, the number of nuclei continuously increases with time. For instantaneous nucleation, provided the total number of platinum

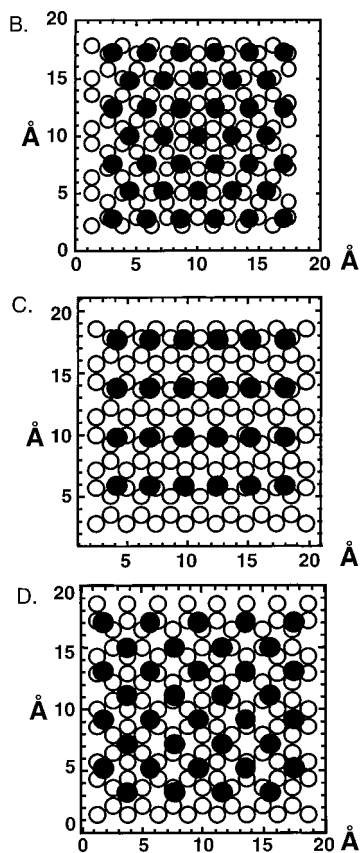
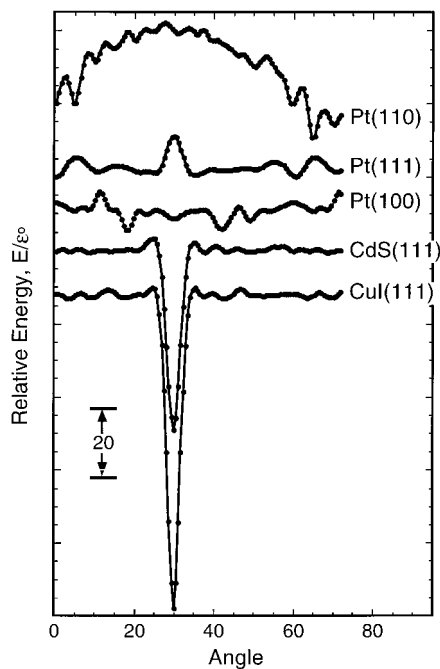


**Figure 9.** Plot of the total energy of a platinum nanocrystal as a function of its azimuthal orientation on a graphite surface calculated using Lennard-Jones 6–12 interaction potentials. Calculations for all three low index planes of the particle in contact with the graphite surface are shown: Also shown for purposes of comparison are calculations for the (111) planes of CuI and CdS in contact with graphite. Previously we have shown that nanocrystals of these two materials adopt epitaxial orientations on the graphite surface corresponding to an azimuthal angle of  $30^\circ$  in this plot.

particles,  $N$ , is constant from experiment to experiment, the height (or radius),  $r$ , of  $N$  identical hemispherical particles should be proportional to the cube root of the deposition charge,  $Q^{1/3}$ ,

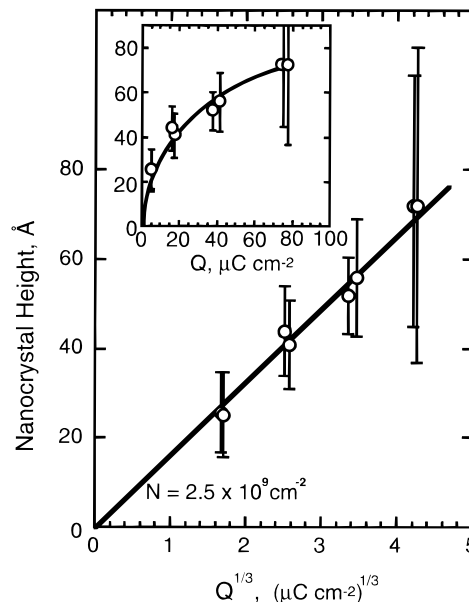


**Figure 10.** Plots of the mean particle height versus charge (inset) and the mean particle height versus charge $^{1/3}$  (i.e.  $Q^{1/3}$ ). The straight line is that expected for a particle density of  $2.3 \times 10^9 \text{ cm}^{-2}$  on each of the surfaces, as described in the text.

and given by the equation

$$r = \left[ \frac{3}{2} \frac{M}{z\pi F \rho N} \right]^{1/3} Q^{1/3} \quad (1)$$

where  $M$  and  $\rho$  are the atomic mass and density of platinum, respectively, and  $z$  is the adsorption electrovalency which is assumed to be 4.0.

The apparent platinum particle height,  $r$ , is plotted versus the deposition charge in Figure 10(inset). Also shown in Figure 10 is a plot of  $r$  versus  $Q^{1/3}$  showing the linear relationship which is observed, qualitatively in accordance with eq 1. The solid line shown in Figure 10 is a fit of eq 1 to the experimental data using a value for the nucleation density,  $N$ , of  $2.3 \times 10^9 \text{ cm}^{-2}$ . This nucleation density is approximately 16% lower than that which was obtained from an analysis of the NC-AFM image data for these surfaces and therefore in good agreement. These data show that  $N$  does not increase appreciably during the pulse durations—from 10 to 100 ms—spanned by the eight experiments represented in this plot and demonstrate conclusively that the nucleation of platinum in this experiment is instantaneous on the 10 ms time scale.

Usually, instantaneous nucleation is observed when deposition conditions allow for very rapid nucleation (i.e., saturation) at defects of a particular type on a heterogeneous surface. One obvious way that this can occur on graphite surfaces is when, at low overpotentials, step edges are selectively decorated.<sup>10</sup> However, for surfaces prepared using large overpotentials, NC-AFM images such as those of Figure 3 show many platinum nanocrystals are located in the middle of terraces on the graphite surface, regions which appear to be atomically smooth and free of defects. If these terraces were, in reality, free of defects, then nucleation would be expected to occur progressively since a large excess of energetically identical sites for nucleation exist on atomically smooth regions of the graphite surface, and the applied potential (i.e., the thermodynamic driving force) remains constant throughout the duration of the deposition pulse. The observation of an instantaneous mechanism for nucleation on the graphite basal plane is one of two pieces of evidence which suggests that discrete defect sites *that are invisible to the NC-*

AFM are present on the terraces of the graphite basal plane. The second piece of evidence involves variations in the nucleation density that are observed from graphite crystal to graphite crystal. Significantly, linear  $r$  versus  $Q^{1/3}$  plots such as that of Figure 10 were only obtained when all platinum nanocrystal samples were prepared on freshly cleaved surfaces of the same piece of graphite. This is because the nucleation density varied systematically by as much as 1 order of magnitude, from  $\approx 10^9$  to  $\approx 10^{10}$   $\text{cm}^{-2}$ , from crystal to crystal. The difference in nucleation density that is intrinsic to different graphite crystals is manifested primarily as a variation in the density of particles on apparently smooth regions of the surface (i.e., terraces) since step edges are always densely covered with platinum particles, even at crystals that show systematically low nucleation densities for platinum on terraces. Taken together, the observations of instantaneous nucleation, and systematic fluctuations of the nucleation density on terraces from crystal to crystal, strongly suggest that the nucleation of platinum nanocrystallites on terraces occurs at defects that are not seen in the NC-AFM imaging experiment. Inspection of the basal plane using scanning tunneling microscopy (STM) and the conventional repulsive mode AFM imaging also failed to reveal the types of point defects on the basal plane that must exist based on the evidence. The nature of these hidden defects is the subject of ongoing investigations in this lab.

Because the growth of platinum nanocrystals on graphite is, itself, electrochemical, it comes as no surprise that these particles are in intimate electrical contact with the graphite surface following deposition. This fact, however, is verified by the voltammetric measurements shown in Figure 11 for platinum dispersions on graphite in aqueous 0.05 M  $\text{H}_2\text{SO}_4$  (all data acquired at 50  $\text{mV s}^{-1}$ ). Three sets of voltammetric data for platinum nanocrystal dispersions are shown in Figure 11 for samples having mean particle diameters of 15 (D), 43 (C), and 155 Å (B). Also shown for purposes of comparison are the responses of a clean, freshly cleaved graphite surface (E) and a clean polycrystalline platinum electrode (A) in this same electrolyte. The first conclusion that can be derived from these data is that large platinum nanocrystals (diameter  $> 120$  Å, see B) exhibit voltammetry that is, in every way, identical with that of a polycrystalline platinum surface. This conclusion provides independent evidence (in addition to the TEM data) of the exposure of (111) and (100) facets at the surface of these nanocrystals. The fact that the ratio between the weakly and strongly adsorbed hydrogen waves (at  $-0.595$  and  $-0.460$  V, respectively) is unchanged from bulk platinum further shows that these two crystalline faces are present on the nanocrystallites in approximately the same proportion as at polished platinum surfaces. The voltammograms C and D for progressively smaller Pt nanocrystals evolve from the bulklike voltammetry of B in two ways: First, the reversible hydrogen adsorption waves that are fully developed at the 155 Å nanocrystals become blurred for Pt particles that are 40–80 Å in diameter and eventually disappear entirely for Pt particles smaller than 30 Å in diameter. Note that for these smallest Pt nanocrystals H-adsorption waves are not recovered by decreasing the negative limit of these voltammetric scans; H-adsorption waves are simply not observed prior to the onset of  $\text{H}_2$  evolution. The second trend involves the quasi-reversible platinum oxide formation and reduction waves (indicated by arrows). The potential difference between these two coupled voltammetric waves,  $\Delta E_p$ , is an indication of the degree of reversibility of oxide formation, and the value of  $\Delta E_p$  increases with decreasing particle size—175 (A, B), 440 (C), and 500 mV (D)—showing

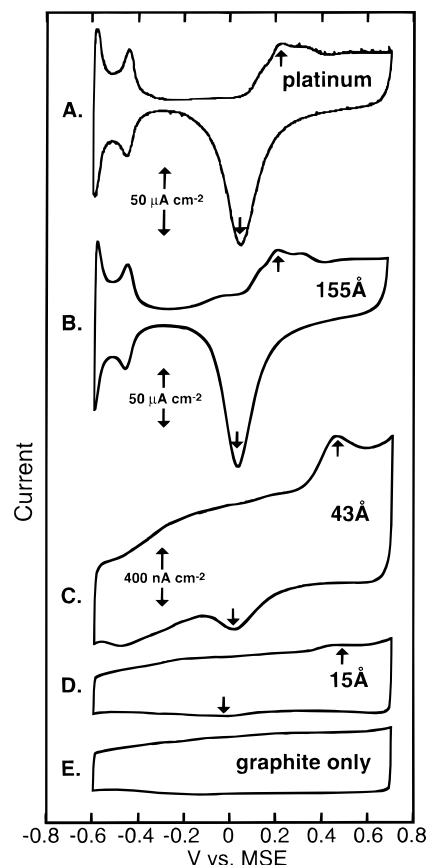


**Figure 11.** Cyclic voltammograms at 50  $\text{mV s}^{-1}$  acquired in aqueous 0.05 M  $\text{H}_2\text{SO}_4$  for five different electrodes as follows: (A) macroscopic platinum wire electrode, (E) freshly cleaved graphite surface with no platinum, (B–D) graphite surfaces on which platinum nanocrystals have been deposited using the method described in this paper. Mean particle diameters for each surface, measured using NC-AFM, are as indicated.

that the platinum oxide formation process becomes less and less reversible as the platinum particle size decreases. In this trend, however, significant scatter exists for the smallest platinum particles, and we have seen 7 Å Pt nanocrystals, for example, which exhibit a  $\Delta E_p$  as small as 420 mV. Neither of these two trends with particle size has been discernible for platinum nanocrystals in previous electrochemical studies.

#### IV. Summary

An electrochemical method for preparing dispersions of platinum nanocrystals on the graphite basal plane has been described. The platinum nanocrystals in these dispersions possess good size monodispersity (for mean diameters  $< 50$  Å), can have mean diameters in the range from 10 to 100 Å, and are well separated from one another on the graphite surface, on average. In addition, it is apparent from electron diffraction measurements that the platinum particles obtained using the pulsed potentiostatic method are not epitaxially aligned with the graphite surface and are air stable for days. Finally, both TEM imaging data and electrochemical studies reveal that both (111) and (100) facets are present on the surfaces of these platinum nanocrystals.

The mechanism of Pt nucleation and growth is readily deduced from these data and is substantially different from mechanisms that have been proposed based, for example, on ex-situ STM investigations of graphite electrode surfaces.<sup>37</sup> Upon the application of the negative potentiostatic pulse shown in Figure 4, platinum nanocrystals nucleate instantaneously (i.e.,

on the microsecond time scale) on the graphite basal plane both at step edges and at point defects on terraces that are not visible to the NC-AFM or STM. These nanocrystals grow by *radial* diffusion control (characterized by linear current versus time<sup>1/2</sup>) for less than 10  $\mu$ s before the diffusion layers from adjacent nanocrystals (which are separated by a few hundred angstroms) coalesce, and an approximately planar diffusion field is generated. The initial radial transport regime is too brief to be detected experimentally, and linear current versus time<sup>-1/2</sup> plots, characteristic of planar diffusion control, are obtained for times as short as  $\approx 20 \mu$ s. A lingering question involves the origin of the broad particle size distributions that emerge from narrow size distributions as Pt nanocrystals grow larger. Using Brownian dynamics simulations, we have recently demonstrated that this broadening of the particle size distribution with the mean particle size is a natural consequence of particle growth in the *planar diffusion control* regime on surfaces where variations in the local areal density of particles are present.

From an applications standpoint, graphite-supported Pt nanocrystal dispersions prepared by this method should provide the best opportunity yet for observations of particle size effects in a variety of technologically important electrocatalysis reactions such as the methanol oxidation and oxygen reduction reactions.

**Acknowledgment.** The financial support of this work was provided by the Office of Naval Research (#N00014-93-1-0757). R.M.P. also acknowledges financial support as an A.P. Sloan Foundation Fellow, a Camille Dreyfus Teacher-Scholar, and an Arnold and Mabel Beckman Foundation Young Investigator. S.G. acknowledges the financial support of a Welch Scholarship of the International Union for Vacuum Science. The authors express their gratitude to Dr. Art Moore of Advanced Ceramics Inc. for the donation of some of the graphite employed for these investigations. Dr. Ralph Nyffenegger, Ms. Becca Stiger, and Dr. Theresa McIntire are also gratefully acknowledged for their technical assistance.

## References and Notes

- (1) Dispersion is defined as the fraction of metal atoms that are exposed at the surface of a deposit.
- (2) Che, M.; Bennett, C. O. *Adv. Catal.* **1989**, *36*, 55.
- (3) Kabbabi, A.; Gloaguen, F.; Andolfato, F.; Durand, R. *J. Electroanal. Chem.* **1994**, *373*, 251.
- (4) Frelink, T.; Visscher, W.; van Veen, J. A. R. *J. Electroanal. Chem.* **1995**, *382*, 65.
- (5) Yahikozawa, K.; Fujii, Y.; Matsuda, Y.; Nishimura, K.; Takasu, Y. *Electrochim. Acta* **1991**, *36*, 973.
- (6) Watanabe, M.; Sei, H.; Stonehart, P. *J. Electroanal. Chem.* **1989**, *261*, 375.
- (7) Takasu, Y.; Ohashi, N.; Zhang, X. G.; Murakami, Y.; Minagawa, H.; Sato, S.; Yahikozawa, K. *Electrochim. Acta* **1996**, *41*, 2595.

- (8) Kinoshita, K. *J. Electrochem. Soc.* **1990**, *137*, 845.
- (9) Zoval, J. V.; Stiger, R. M.; Biernacki, P. R.; Penner, R. M. *J. Phys. Chem.* **1996**, *100*, 837.
- (10) Zoval, J. V.; Biernacki, P.; Penner, R. M. *Anal. Chem.* **1996**, *68*, 1585.
- (11) Hsiao, G.; Anderson, M. G.; Gorer, S.; Harris, D.; Penner, R. M. *J. Am. Chem. Soc.*, in press.
- (12) Anderson, M.; Gorer, S.; Penner, R. M. *J. Phys. Chem. B* **1997**, *101*, 5895.
- (13) Grabar, K. C.; Smith, P. C.; Musick, M. D.; Davis, J. A.; Walter, D. G.; Jackson, M. A.; Guthrie, A. P.; Natan, M. J. *J. Am. Chem. Soc.* **1996**, *118*, 1148.
- (14) Grabar, K. C.; Freeman, R. G.; Hommer, M. B.; Natan, M. J. *Anal. Chem.* **1995**, *34*, 735.
- (15) Chao, L.; Andres, R. P. *J. Colloid Interface Sci.* **1994**, *165*, 290.
- (16) Freeman, R. G.; Grabar, K. C.; Allison, K. J.; Bright, R. M.; Davis, J. A.; Guthrie, A. P.; Hommer, M. B.; Jackson, M. A.; Smith, P. C.; Walter, D. G.; Natan, M. J. *Science* **1995**, *267*, 1629.
- (17) Baker, B. E.; Kline, N. J.; Treado, P. J.; Natan, M. J. *J. Am. Chem. Soc.* **1996**, *118*, 8721.
- (18) Teranishi, T.; Hosoe, M.; Miyake, M. *Adv. Mater.* **1997**, *9*, 65.
- (19) Shaikhutdinov, S. K.; Möller, F. A.; Mestl, G.; Behn, R. J. *J. Catal.* **1996**, *163*, 492.
- (20) Giersig, M.; Mulvaney, P. *Langmuir* **1993**, *9*, 3408.
- (21) Gillet, M.; Renou, A. *Surf. Sci.* **1979**, *90*, 91.
- (22) Röder, H.; Hahn, E.; Brune, H.; Bucher, J.-P.; Kern, K. *Nature* **1993**, *366*, 141.
- (23) Bartholomew, C. H.; Boudart, M. *J. Catal.* **1972**, *25*, 173.
- (24) Aika, K.; Ban, L. L.; Okura, I.; Namba, S.; Turkevich, J. *J. Res. Inst. Catal., Hokkaido Univ.* **1976**, *24*, 54.
- (25) Henglein, A.; Ershov, B. G.; Malow, M. *J. Phys. Chem.* **1995**, *99*, 14129.
- (26) Rampino, L. D.; Nord, F. F. *J. Am. Chem. Soc.* **1941**, *63*, 2745.
- (27) Ahmadi, T. S.; Wang, Z. L.; Henglein, A.; El-Sayed, M. A. *Chem. Mater.* **1996**, *8*, 1161.
- (28) Shimazu, K.; Weisshaar, D.; Kuwana, T. *J. Electroanal. Chem.* **1987**, *233*, 223.
- (29) Georgolios, N.; Jannakoudakis, D.; Karabinas, P. *J. Electroanal. Chem.* **1989**, *264*, 235.
- (30) Wang, J.; Golden, T.; Lin, Y.; Angnes, L. *J. Electroanal. Chem.* **1992**, *333*, 65.
- (31) Zuburtikudis, I.; Saltsburg, H. *Science* **1992**, *258*, 1337.
- (32) Allongue, P.; Souteyrand, E. *J. Electroanal. Chem.* **1993**, *362*, 79.
- (33) Cachet, H.; Froment, M.; Souteyrand, E.; Dennig, C. *J. Electrochem. Soc.* **1992**, *139*, 2920.
- (34) Reetz, M. T.; Helbig, W. *J. Am. Chem. Soc.* **1994**, *116*, 7401.
- (35) Mizukami, F.; Taniguchi, F.; Kiyozumi, Y.; Kobayashi, A.; Izutsu, H.; Maeda, K. *Adv. Mater.* **1994**, *6*, 856.
- (36) Bard, A. J.; Faulkner, L. R. *Electrochemical Methods: Fundamentals and Applications*; John Wiley and Sons: New York, 1980.
- (37) Zubimendi, J. L.; Vazquez, L.; Ocon, P.; Vara, J. M.; Triaca, W. E.; Salvarezza, R. C.; Arvia, A. J. *J. Phys. Chem.* **1993**, *97*, 5095.
- (38) *The Fundamentals of Metal Deposition*; Harrison, J. A., Thirsk, H. R., Eds.; Marcel Dekker: New York, 1971; Vol. 5.
- (39) Gunawardena, G.; Hills, G.; Montenegro, I.; Scharifker, B. J. *J. Electroanal. Chem.* **1982**, *138*, 225.
- (40) Hoare, M. R.; Pal, P. *J. Cryst. Growth* **1972**, *17*, 77.
- (41) Yacaman, M. J.; Dominguez, J. M. *J. Catal.* **1980**, *64*, 213.
- (42) Dominguez, J. M.; Yacaman, M. J. *J. Catal.* **1980**, *64*, 223.